MODELLING OF TRANSPORT PROCESSES IN CONCRETE EXPOSED TO ELEVATED TEMPERATURES – AN ALTERNATIVE FORMULATION FOR SORPTION ISOTHERMS

C. T. Davie[1*], C. J. Pearce[2], K. Kukla[2] and N. Bićanić[2]

[1] *School of Civil Engineering and Geosciences, Newcastle University, Newcastle upon Tyne, UK*

[2] *School of Engineering, University of Glasgow, Glasgow, U.K.*

*Correspondence to:

Colin T Davie

School of Civil Engineering and Geosciences,

Newcastle University

Newcastle upon Tyne,

NE1 7RU, United Kingdom

Email: colin.davie@ncl.ac.uk

Telephone: +44-(0)191 208 6458

Keywords: Transport Properties (C), Adsorption (C), Temperature (A), Modeling (E)

Abstract

There is a significant need to understand, analyse and assess moisture transport in cementitious materials exposed to elevated temperatures in order to confidently predict the behaviour and ultimately the development of damage in safety critical applications such as nuclear reactor vessels, structures exposed to fire and well bore grouts.

In view of this need a rigorous and robust formulation to describe water retention curves (sorption isotherms) as a function of temperature based on the evolution of physical parameters is presented. The model formulation is successfully validated against independent sets of experimental data up to temperatures of 80°C. It is then further validated under isothermal drying conditions and then high temperature conditions through the numerical reproduction of laboratory experiments following implementation in a fully coupled hygro-thermo-mechanical finite element model.

The new formulation is found to work well under a variety of conditions in a variety of cementitious material types.

1. Introduction

It has long been identified that pore pressures and moisture movement are critical in the prediction of damage to cementitious materials exposed to elevated temperatures, including those in nuclear reactor vessels, structures exposed to fire and well bore grouts [1].

With the ever increasing demand for energy worldwide and the threat of global warming, nuclear power is experiencing a resurgence in popularity with several countries looking again to it as a reliable, plentiful and low carbon supply of electricity [2, 3] including China, India and the UK recently approving the development of new-build plants [2]. Similarly, despite recent economic concerns, oil and gas exploration remains an import component in global energy supplies. However, with continued concerns over the safety of nuclear power plants (following events such as those at the Fukushima Dai-ichi plant in Japan, where a loss of cooling led to the overheating of several reactors and the release of radioactive material [4]), with incidents such as the Deepwater Horizon fire (where a blow out in the well led to a fatal fire and major environmental consequences [5]) and with continuing threats from militant groups and terrorists, understanding damage to these safety critical structures is ever more important. Thus the need for robust methods of analysis that

can account for pore pressures and moisture movement in these structures at elevated temperatures is ever more critical. This work addresses this need directly.

2. Current Models for Moisture Movement

There has been significant development of numerical models for concrete at elevated temperatures over the last several decades [1, 6-13] and these have now evolved to highly sophisticated coupled models taking into account hygro-thermo-(chemo)-mechanical behaviour of multi-phase processes in the concrete. However, the majority of these models act at the macro-scale (typically necessary for the consideration of structural components or whole buildings) and so tend to lack detailed formulations for some key aspects of behaviour taking place at smaller scales inside the concrete material. They instead rely on phenomenological models at the macro-scale to capture and account for processes occurring at the micro- and meso-scales.

One of the critical areas for consideration in this kind of problem is the moisture content in the complex, irregular pore structure of the concrete. Without detailed consideration of multi-scale behaviour (which would add significant further complexity to already complex models and the science for which is still in early stages of development and research), a key state equation required for these macro-scale models is the sorption isotherm (also often known as the water retention curve in soil mechanics). For a homogenised continuum, representing the true medium, these curves relate the statistical average water content to relative humidity and may be variously formulated in terms of saturation, gravimetric water content or volumetric water content vs. suction, capillary pressure or relative humidity (all of which are related to each other via the Kelvin-Laplace Equation [7])

$$\ln\frac{P_V}{P_{Sat}} = \ln h = \frac{2\gamma V_m}{rRT} = -\frac{P_C}{\rho_L R_V T} \tag{1}$$

where, P_V is the partial vapour pressure, P_{Sat} is the saturation vapour pressure (so that $h = \frac{P_V}{P_{Sat}}$ is the relative humidity), γ is the surface tension, V_m is the molar volume, r is the radius of curvature, R is the ideal gas constant, T is the temperature, P_C is the capillary pressure, ρ_L is the density of water & R_V is the gas constant for water vapour.

Unfortunately very little information exists in the literature in relation to such curves for concrete, especially when it must be considered that they are strongly temperature-dependent up to the critical point for water as well as being functions of the material properties.

Many existing state-of-the-art models rely on Bažant's formulation, originally developed in the 1970s [1], e.g. [10, 11, 13, 14]. Although these curves provide a reasonable approximation with which these models can work, there are a number of issues that mean they are no longer ideal for the purpose. Firstly, although they account for concrete type (and the inherent effects of micro-structural differences) to a certain extent by including cement content in their formulation, this has only a limited effect [11] and it is noted that they are designed, semi-empirically, for normal-strength concrete and are not necessarily suitable for the dense, high-performance concretes often used today and likely to be used in new-build nuclear plants [15]. Secondly, the curves were originally formulated in consideration of total moisture content rather than separate liquid and vapour phases. Where state-of-the-art models have evolved to consider multiple phases of water, adaptations have had to be made based on interpretation of Bažant's work. Finally, the discontinuous nature of the curves presents some challenges when implementing them numerically and further adaptations of the original formulation are often required to provide a smoothed transition function at higher relative humidity [10, 11].

3. Isotherm Formulation

To address the issues described above consideration is given here to the work of Poyet [16] and more particularly to the work of Baroghel-Bouny et al. [17] both of whom found the van Genuchten equation [18] to provide a good model for isotherms in cementitious materials (both cement pastes and concretes).

Baroghel-Bouny et al. presented an experimentally derived function for capillary suction vs. degree of saturation with liquid water at ambient temperature suitable for both normal and high-strength concretes and Poyet developed a temperature-dependent model that successfully fits the experimental results of several other Authors up to 80°C.

Poyet's model, which is purely based on a fitting of the experimental results with an extrapolation based on the van Genuchten model parameters, has the advantage of being simple but is found to be limited by its formulation to temperatures <115°C; too low to be of

use in addressing fire or Fukushima type incidents. As an alternative, this work uses the curve of Baroghel-Bouny et al. as a starting point and adopts the work of Leverett [19] to develop a model based on the evolution of material properties with temperature (independently determined elsewhere). As a mathematical function it is unrestricted in temperature range and does not wholly rely on fitting to experimental isotherm results to define its parameters.

Baroghel-Bouny et al. presented their ambient temperature curve as shown in

$$P_C = a(S^{-b} - 1)^{1-\frac{1}{b}} \tag{2}$$

where, P_C is the capillary suction, S is the degree of saturation with liquid water at 20°C and a & b are material constants that vary depending on the concrete mix (See Table 1). It may be noted that a is equivalent to the parameter α described by van Genuchten with units of pressure (Pa) and b is a dimensionless parameter equivalent to $1/m$ in van Genuchten's notation.

Table 1. Model parameters for normal-strength and high-strength concretes [17]

	Mix	
Parameter	NSC	HSC
a (MPa)	18.6237	46.9364
b	2.2748	2.0601

To extrapolate this curve for elevated temperatures we now consider the work of Leverett [19]. Leverett showed that at ambient temperatures a dimensionless empirical relationship, J, exists between the degree of saturation with liquid water and the capillary suction, as a function of the micro-structure of the material (characterised by the porosity and the permeability), which in turn controls the curvature of the capillary menisci of the pore fluid

$$J(S) = \frac{P_C}{\gamma_0}\sqrt{\frac{K_0}{\phi_0}} \tag{3}$$

where γ is the surface tension of the pore fluid, K is the intrinsic permeability, ϕ is the porosity and the sub-script 0 indicates the value at ambient conditions. The relationship $\sqrt{\frac{K}{\phi}}$

can be considered as a characteristic length for the material and an estimate of the mean hydraulic radius of the pore throats.

For the Baroghel-Bouny curve (2), the equivalent *J*-curve can therefore be expressed as

$$J_{BB}(S) = \frac{a(S^{-b}-1)^{1-\frac{1}{b}}}{\gamma_0}\sqrt{\frac{K_0}{\phi_0}} \tag{4}$$

Considering again Leverett's *J*-curve (3) it may be noted that the material properties are all functions of temperature [11, 15] such that, with rearrangement, the capillary suction may be expressed as a function of saturation with liquid water and temperature

$$P_C(S,T) = J(S)\gamma(T)\sqrt{\frac{\phi(T)}{K(T)}} \tag{5}$$

That the micro-structure of cementitious materials evolves with increase temperature is well known [15] and corresponds with the premise of $\sqrt{\frac{\phi(T)}{K(T)}}$ in (5). Assuming here that, for any fixed temperature, an equilibrium relationship exists between the micro-structure of the material at that temperature and the curvature of the capillary menisci then, if the porosity and permeability are known and the effects of temperature on the pore fluid are accounted for, a *J*-curve can be defined. I.e. concrete at a given temperature can be considered as any other porous material, with a specific micro-structure and containing a pore fluid with specific properties.

Thus, by combining (4) and (5) we can develop a temperature-dependent set of isotherms based on the isothermal Baroghel-Bouny curve, where changes in the capillary suction with temperature are a result of the temperature-dependent changes to the properties of the liquid water and to the micro-structure of the concrete (i.e. the evolution of the characteristic length)

$$P_C(S,T) = J_{BB}(S)\gamma(T)\sqrt{\frac{\phi(T)}{K(T)}} = \left(\frac{a(S^{-b}-1)^{1-\frac{1}{b}}}{\gamma_0}\sqrt{\frac{K_0}{\phi_0}}\right)\gamma(T)\sqrt{\frac{\phi(T)}{K(T)}} \tag{6}$$

Grouping terms, equation (6) can be written as (7), which it may be noted reduces to (2) for the case of ambient conditions ($\gamma=\gamma_0$, $K=K_0$, $\phi=\phi_0$).

$$P_C(S,T) = a(S^{-b} - 1)^{1-\frac{1}{b}} \cdot \frac{\gamma(T)}{\gamma_0} \cdot \sqrt{\frac{K_0}{\phi_0}} \sqrt{\frac{\phi(T)}{K(T)}} \tag{7}$$

As discussed in section 2 the isotherms can be expressed in a number of different ways. For convenience in comparing results, equation (7) is here rearranged in terms of the saturation

$$S(P_C,T) = \left[\left(\frac{1}{a} \cdot P_C \cdot \frac{\gamma_0}{\gamma(T)} \cdot \sqrt{\frac{\phi_0}{K_0}} \cdot \sqrt{\frac{K(T)}{\phi(T)}} \right)^{\frac{1}{1-\frac{1}{b}}} + 1 \right]^{-\frac{1}{b}} \tag{8}$$

Finally, introducing the Kelvin-Laplace definition for capillary suction (1), allows (8) to be expressed as a function of the relative humidity, *h*

$$S(h,T) = \left[\left(-\frac{1}{a} \cdot R_V T \rho_L(T) \ln(h) \cdot \frac{\gamma_0}{\gamma(T)} \cdot \sqrt{\frac{\phi_0}{K_0}} \cdot \sqrt{\frac{K(T)}{\phi(T)}} \right)^{\frac{1}{1-\frac{1}{b}}} + 1 \right]^{-\frac{1}{b}} \tag{9}$$

To complete the model, temperature-dependent functions are required for the water properties of density, $\rho_L(T)$ & surface tension, $\gamma(T)$, and the concrete material parameters of porosity, $\phi(T)$ & permeability, $K(T)$.

The temperature dependence of water density is well known and can be described by e.g. Furbish's equation [20]. The temperature dependence of surface tension is similarly well known (e.g. IAPWS-95 formulation [21]) and can be described by a polynomial fitted to the data using a least-squares approach.

$$AT^6 - BT^5 + CT^4 - DT^3 + ET^2 - FT + G \tag{10}$$

where $A = 3.55002752446469\times10^{-17}$, $B = 9.07297190676255\times10^{-14}$, $C = 9.60574133604685\times10^{-11}$, $D = 5.35106618941698\times10^{-8}$, $E = 1.62314916432718\times10^{-5}$, $F = 2.66341044436865\times10^{-3}$, $G = 2.71175300176033\times10^{-3}$ and T is in Kelvin.

Porosity in concrete has been shown to increase three-fold between 100°C and 800°C [22] and following Tenchev et al. [10] this is described here by a cubic function of temperature

$$\phi = \phi_0 \times \begin{cases} 1 & \text{for } (T < 100℃) \\ pT^3 + qT^2 + rT + s & \text{for } (100℃ \leq T \leq 800℃) \\ 3 & \text{for } (T > 800℃) \end{cases} \quad (11)$$

where, p, q, r & s are fixed coefficients of a cubic function such that $\phi(T)$ and its derivative, $\frac{d\phi}{dT}$, are continuous as ϕ evolves from ϕ_0 to $3\phi_0$.

Permeability has been variously described for cementitious materials both directly and indirectly as a function of temperature, e.g. [23]. In order to compare the performance of this model with experimental data for cement pastes as consistently as possible in the first instance the permeability function back-calculated by Drouet et al. [24] from their results is employed here in the first instance

$$K(T) = K_0 \exp\left[\exp\left(\frac{T-293.15}{T_c}\right) - 1\right] \quad (12)$$

where, T_c is a material coefficient, with values taken directly from [24].

Examining equation (9) it can be seen that there are four factors that control the evolution of the shape of the isotherms with temperature. Three of these; the temperature (T), density of water ($\rho_L(T)$) and surface tension (strictly, the inverse ratio to its ambient value ($\frac{\gamma_0}{\gamma(T)}$)), are all physically related to the properties of the water and control the way in which the water forms menisci with increasing temperatures. Thus, for a given saturation in the porous structure of the concrete, all of these will affect the equilibrium state between liquid water and water vapour. The fourth factor; the ratio of Leverett's characteristic length to its ambient value ($\sqrt{\frac{\phi_0}{K_0}} \cdot \sqrt{\frac{K(T)}{\phi(T)}}$), reflects the physical changes in the pore structure as a result of the temperature increase. Likewise, this will affect the geometry of the menisci formed and hence will change the equilibrium state.

These effects are then reflected in the form of the isotherms as can be seen in Figure 1 where an example set of curves is shown. These isotherms are developed for 20°C, 50°C & 80°C using equation (9) with parameter values a & b for NSC (Table 1) and populated with Furbish's equation [20] to describe the density of water, plus equations (10), (11) & (12) respectively describing the evolutions of surface tension, porosity and permeability.

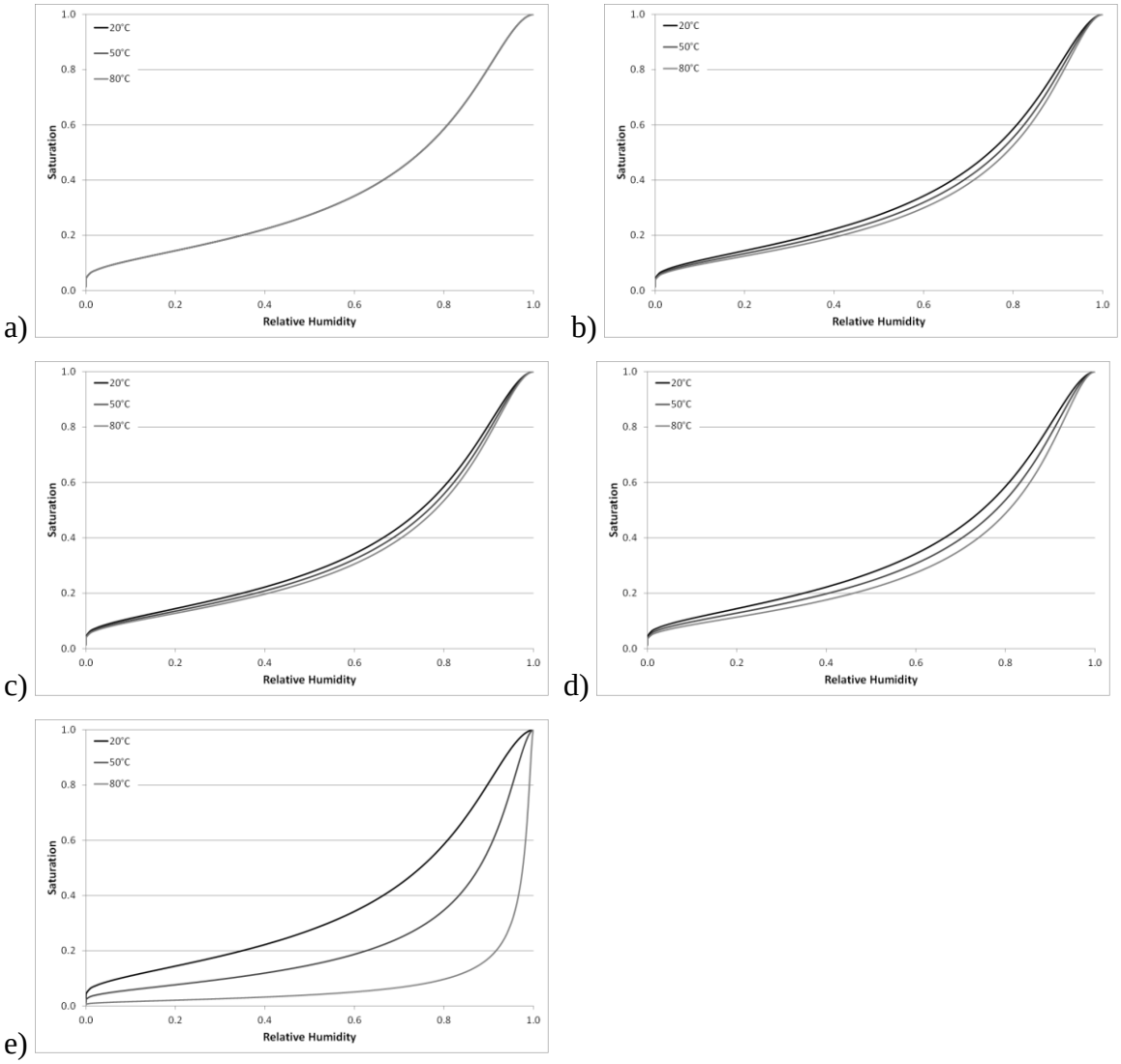

Figure 1 Effects of temperature dependent properties on example isotherm (9) showing a) isothermal conditions b) temperature c) density of water d) surface tension e) pore structure (Leverett's characteristic length)

Figure 1a shows the isotherms with all four factors held constant, i.e. no thermal dependencies, and as would be expected all three lines overlap. The influence of each of the thermally dependent water properties can then be seen as they are introduced one at a time in Figures 1b-d. Introducing temperature (Figure 1b) spaces the lines out slightly to the right (i.e. the equilibrium state requires higher relative humidity for a given saturation, suggesting an increase in the radii of the menisci and a decrease in capillary pressure). When the thermal effects on density are introduced (Figure 1c) there is only a very small effect and the equilibrium state in fact moves back slightly left (i.e. reducing relative humidity, increasing capillary pressure as a result of decreasing curvature). Introducing the thermal dependence of

surface tension (Figure 1d) spaces the lines further to the right again (increasing relative humidity, decreasing capillary pressure as a result of decreasing curvatures which is physically consistent with the reduction in the surface tension), but again the effect is not large. Finally, introducing the effects of temperature on the characteristic length, and thus on pore structure (Figure 1e), can be seen to have the largest effect of all, spacing the lines significantly to the right (i.e. increasing relative humidity, decreasing capillary pressure which again in physically consistent with a decrease in the radii of the menisci as the pore structure opens up). Clearly, and as will be apparent later, this depends on the way in which the porosity and permeability increase relative to each other. However, the effect of the pore structure is always likely to be more significant than the effect of the properties of the water.

4. Model Validation

The new formulation was validated against the experimental results of Drouet et al. [24], Ishida et al. [25] and Brue et al. [26] as presented by Poyet [16]. Using the formulation described in the previous section plots of saturation against relative humidity were produced for each of seven separate data sets (Figure 2a-g). The initial (20°C) curve from which the isotherms evolve, was in each case defined using the appropriate values for the material parameters (a & b) either from [24] (Figure 2a-d) or as required to reproduce 20°C curves presented by Poyet [16] (Figure 2e-g). The curves at higher temperatures were produced using the isotherm formulation derived in (9) populated with the independently derived functions for density, surface tension, porosity and permeability as described above. No parametric tuning was involved. For comparison the curves predicted by the model are shown against the experimental data and best fit curves.

As can be seen from Figure 1 the model fits well and reasonably close to the best fit curves across all of the materials considered, which includes results for a range of cement paste types and concretes from several independent studies, over a range of temperatures up to 80°C. The model seems to fit best the higher temperatures (60°C & 80°C) and slightly less well against the mid-temperatures (40°C & 50°C) where it tends to over predict saturation, although by never more than about 0.08 in the examples considered. This is generally the same trend as found by Poyet [16] for his model but it may also be seen that this model provides closer fits in a number of cases.

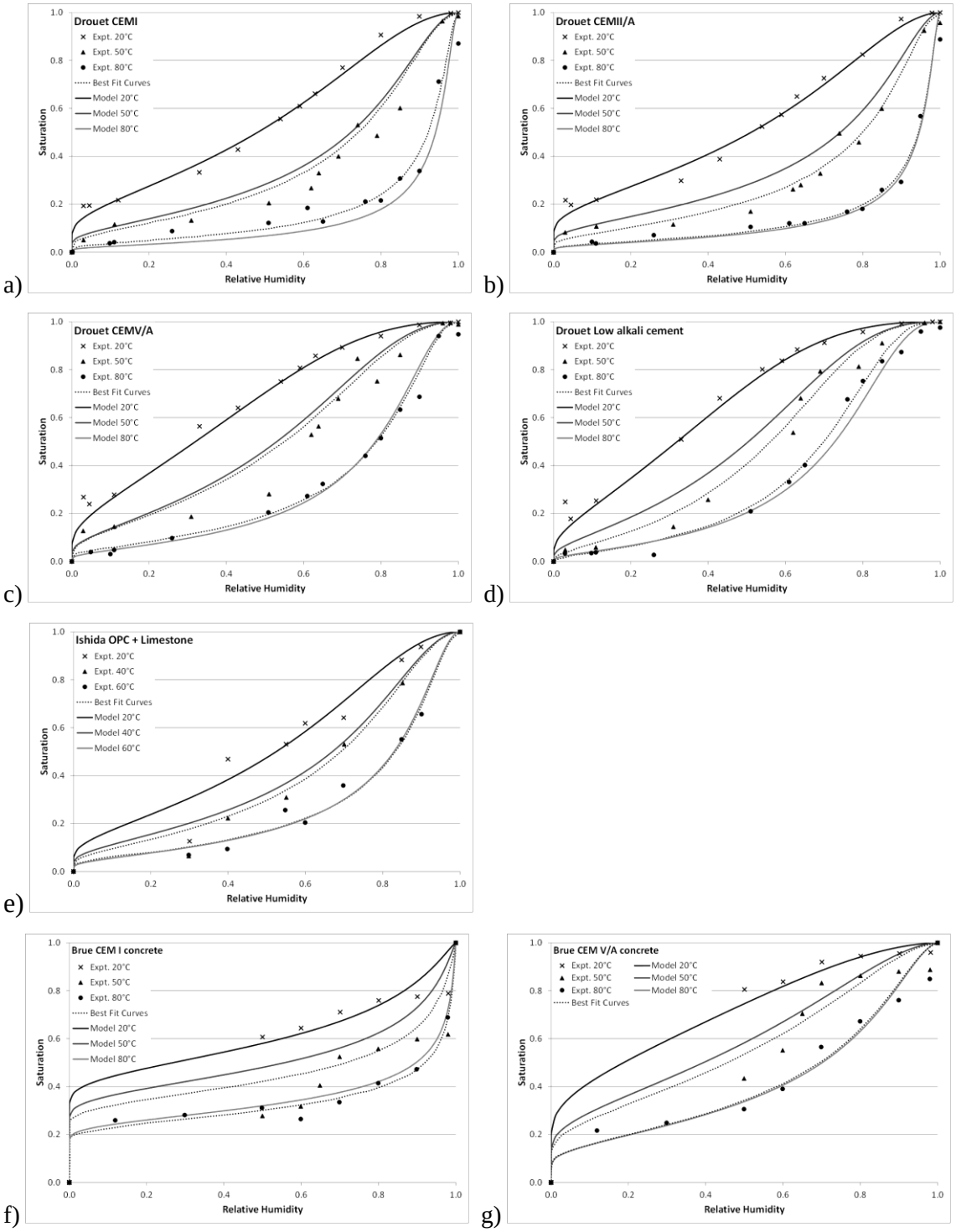

Figure 2 Comparison between the new isotherm formulation and the experimental results of Drouet et al. [24] (a-d), Ishida et al. [25] (e) and Brue et al. [26] (f-g)

It may be noted that when considering saturation, where the effect of porosity is diminished through normalisation, the permeability as a function of temperature remains significant in determining the evolution of the isotherm. However, in order to extend the model to high temperatures the permeability function developed by Drouet et al. [24] (12) cannot be

practically used since it quickly predicts extreme values for permeabilities (7.5×10^{44}m^2@200°C).

As an alternative the permeability function (12) is replaced here with that proposed by Bary (cited by Gawin et al. [27]) which describes the permeability as an exponential function of damage, i.e. changes to the micro-structure resulting from thermal and/or mechanical loading

$$K = K_0 \times 10^{A_D D} \tag{13}$$

where, A_D is a material coefficient and D is the damage described in the context of a classical isotropic elastic-damage model modified to include the effects of both thermal and mechanical damage such that $D = 1-(1-\omega)(1-\chi)$ where ω is the mechanical damage parameter and χ is the thermal damage parameter [11, 27].

Neglecting for the moment mechanical effects not present in these experimental results (i.e. $\omega = 0$) and considering thermal effects only, the damage caused by heating can be described according to Nielsen et al. [28] by[1]

$$\chi = 2 \times 10^{-3}(T - T_0) - 1 \times 10^{-6}(T - T_0)^2 \tag{14}$$

Implementing this function for damage (14), with $\omega = 0$, within Bary's formulation for permeability (13) gives

$$\begin{aligned} K &= K_0 \times 10^{A_D\left(1-(1-\omega)(1-\chi)\right)} \\ &= K_0 \times 10^{A_D(\chi)} \\ &= K_0 \times 10^{A_D\left(2\times10^{-3}(T-T_0)-1\times10^{-6}(T-T_0)^2\right)} \end{aligned} \tag{15}$$

This type of curve has been employed widely in the literature [23, 27, 29] and can be seen here to fit well (with tuning of the material coefficient, A_D) to independent experimental measurements of permeability up to high temperatures (Figure 3a). This is in contrast to the Drouet permeability curve (12), also shown for the same data, which clearly does not have an

[1] NB. Although only thermal effects are considered here, it may be noted that an added advantage of employing Bary's formulation may be that any changes to the isotherm that might result from mechanically induced changes to the micro-structure could be inherently captured along with thermal effects.

appropriate trend over the full temperature range and tends to significantly over predict permeabilities at higher temperatures.

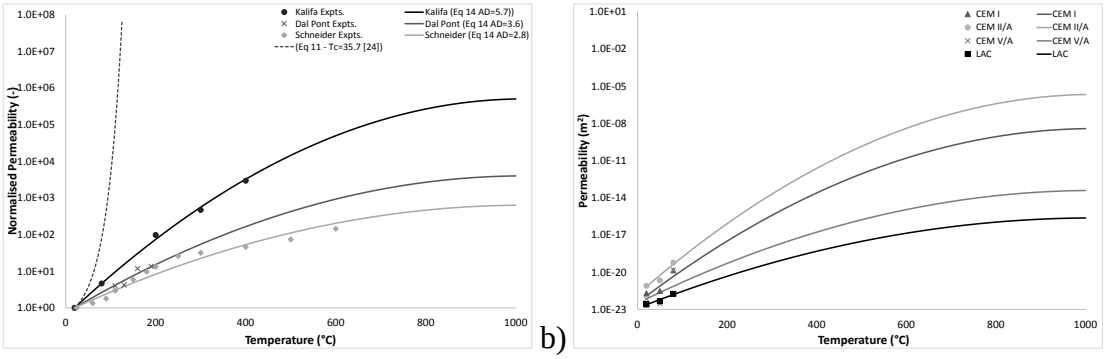

a) b)

Figure 3 a) normalised permeability curves showing the fit of the Drouet (12) and Bary (15) curves tuned to three independent sets of experimental permeability measurements [29-31], b) permeability curves predicted by the Drouet (12) and Bary (15) curves for four cement types with accompanying low temperature permeability results from Drouet et al. [24, 29-31]

Employing (15) in the isotherm formulation instead of (12) and tuning the material coefficient A_D (Table 2) leads to the saturation curves shown in Figure 4.

Table 2 Values of the material coefficient, A_D, required to tune the Bary permeability curve (15) such that a good fit is achieved in the isotherm plots

Material	Material coefficient, A_D
Drouet CEMI	13.5
Drouet CEMII/A	15.5
Drouet CEMV/A	8.75
Drouet LAC	7.0
Ishida OPC + Limestone	11.25
Brue CEMI concrete	18.0
Brue CEMV/A concrete	9.0

As can be seen, this formulation of the model provides some extremely good fits to the higher temperature data (60/80°C) with a general improvement over the results shown in Figure 2. Importantly, in most cases it also provides a better prediction of the evolution from initial conditions (20°C) through mid- (40/50°C) to higher temperatures (60/80°C) and is particularly representative for the concrete materials presented by Brue et al. [26]. As a trend

this formulation tends to very slightly under predict saturation at mid- temperatures, although by never more than about 0.06 in the examples considered here.

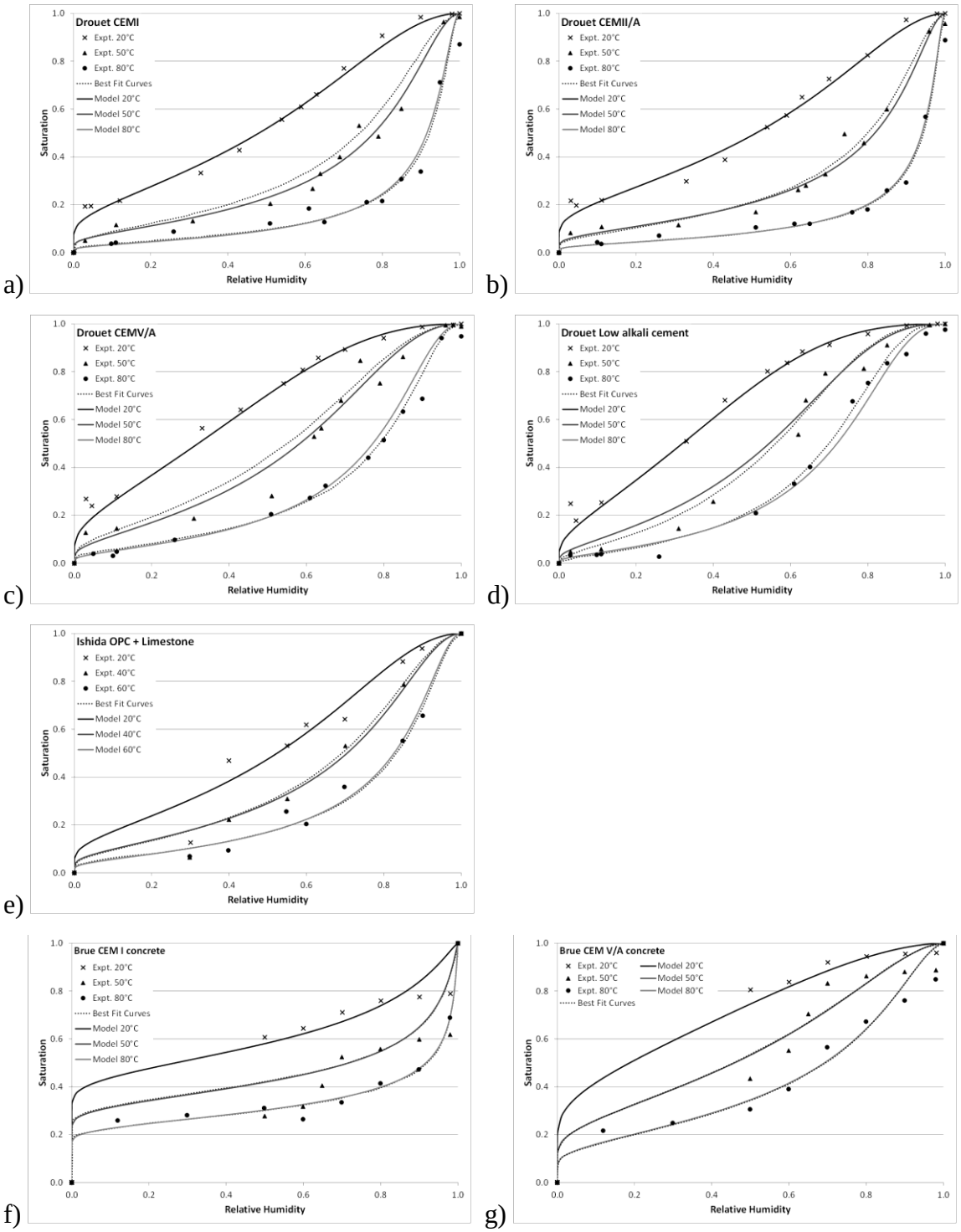

Figure 4 Comparison between the new isotherm formulation including an updated permeability function and the experimental results of Drouet et al. [24] (a-d), Ishida et al. [25] (e) and Brue et al. [26] (f-g)

As an independent check, the permeability curves corresponding to the tuned values of A_D (Table 2) for the first four for these materials are shown in Figure 3b and can be seen to give a reasonable fit with the values of permeability reported by Drouet et al. [24] and Poyet [16] for temperatures up to 80°C. The independent fit of the permeability results plus the isotherm fits gives confidence in the formulation as it is extended and applied to high temperature concrete applications.

5. Numerical Application

Given the need to study cementitious materials at high or very high temperatures and given the lack of experimental results for isotherms above ~80°C an alternative approach is required to build on the confidence developed in the model above and support its use in the wider field. Therefore, to further demonstrate the performance of the new formulation at high temperatures in various materials two sets of numerical analyses were conducted. The first reproduced isothermal drying experiments conducted by Baroghel-Bouny et al. [17] and provide a point of reference for the model implementation and its performance in capturing transient, multi-phase conditions at ambient temperatures. The second reproduced high temperature experiments conducted by Kalifa et al. [32] and demonstrate the model's abilities at high temperatures.

To carry out the analyses the isotherm formulation was implemented within the existing generalised hygro-thermo-mechanical finite element model presented by Davie et al. [11].

5.1. Numerical Implementation

A brief description of the governing and transport equations of the model are given below while a full description of the formulation and implementation as well as auxiliary functions may be found in [11] and [33].

The model considers concrete as a multiphase porous medium consisting of solid, liquid and gas phases. The solid phase is considered to be linear elastic with nonlinear responses to mechanical and thermal loadings accounted for by an isotropic damage formulation. The 'liquid' phase accounts for free liquid water in the pore space, water derived by dehydration from the solid phase and adsorbed water physically bound to solid phase. The gas phase is

considered to be an ideal mixture of dry air and water vapour. The material properties are typically directly or indirectly functions of temperature.

5.1.1. Governing Equations

The governing equations defining the conservations of mass of dry air (16), mass of moisture (17), energy (18) and linear momentum (19) are defined as follows

$$\frac{(\varepsilon_G \tilde{\rho}_A)}{\partial t} = -\nabla \cdot \mathbf{J}_A \tag{16}$$

$$\frac{(\varepsilon_G \tilde{\rho}_V)}{\partial t} + \frac{(\varepsilon_L \rho_L)}{\partial t} - \frac{(\varepsilon_D \rho_L)}{\partial t} = -\nabla \cdot (\mathbf{J}_V + \mathbf{J}_L) \tag{17}$$

$$\left(\underline{\rho C}\right)\frac{\partial T}{\partial t} - \lambda_E \frac{\partial(\varepsilon_L \rho_L)}{\partial t} + (\lambda_D + \lambda_E)\frac{(\varepsilon_D \rho_L)}{\partial t} = -\nabla \cdot (k \nabla T) + \lambda_E \nabla \cdot \mathbf{J}_L \tag{18}$$

$$\nabla \cdot (\sigma' - \eta P_{Pore}\mathbf{I}) + \mathbf{b} = 0 \tag{19}$$

where, ε_θ is the volume fraction of a phase θ (θ = *L, V, A, G, D* refer to liquid water, water vapour, dry air, gas mixture and dehydrated water phases, respectively), ρ_θ is the density of a phase θ, $\tilde{\rho}_\theta$ the mass of a phase θ per unit volume of gaseous material, $\mathbf{J}_\theta$ the mass flux of a phase θ, $\underline{\rho C}$ the heat capacity of concrete, k the effective thermal conductivity of concrete, λ_E and λ_D are the specific enthalpies of evaporation and dehydration, T is the temperature, $\boldsymbol{\sigma'}$ is the Bishop's stress, $\mathbf{I}$ is the identity matrix, η is the Biot coefficient, P_{Pore} is the pore pressure, $\mathbf{b}$ is the body force and t is time.

5.1.2. Fluid Transport Equations

Fluids are assumed to flow through the pore structure under pressure according to Darcy's law. Diffusion of the gas phase according to Fick's law is also considered. The mass fluxes of dry air, water vapour and liquid water are then given by

$$\mathbf{J}_A = \varepsilon_G \tilde{\rho}_A \left(-\frac{k_g K K_G}{\mu_G}\right)\nabla P_G - \varepsilon_G \tilde{\rho}_G D_{AV} \nabla\left(\frac{\tilde{\rho}_A}{\tilde{\rho}_G}\right) \tag{20}$$

$$\mathbf{J}_V = \varepsilon_G \tilde{\rho}_V \left(-\frac{k_g K K_G}{\mu_G}\right)\nabla P_G - \varepsilon_G \tilde{\rho}_G D_{AV} \nabla\left(\frac{\tilde{\rho}_V}{\tilde{\rho}_G}\right) \tag{21}$$

$$\mathbf{J}_L = \varepsilon_L \rho_L \left(-\frac{k_g K K_G}{\mu_G}\right)\nabla P_L \tag{22}$$

where, K is the intrinsic permeability of the concrete, K_θ, μ_θ and P_θ are the relative permeability, dynamic viscosity and pressure of the phase θ, k_g is the gas-slip factor and D_{AV} is the coefficient of diffusion for the dry air/water vapour mixture.

For consideration of flow and mechanical stresses, capillary suctions, P_C, are considered via a rearrangement of the Kelvin Equation

$$P_L = P_G - P_C, \text{ where } P_C = \begin{cases} -R_V T \rho_L \ln\left(\frac{P_V}{P_{Sat}}\right) & \text{for } S > S_{SSP} \\ 0 & \text{for } S \leq S_{SSP} \end{cases} \quad (23)$$

where, S is the degree of saturation with liquid water and S_{SSP} is the solid saturation point, which is the degree of saturation below which all water exists as adsorbed water, physically bound to the concrete skeleton [7].

The last component of the formulation is the liquid water content in the concrete, which can be described in terms of the saturation with liquid water and this is calculated from the sorption isotherms, which have the general form

$$S = f(A, B(T), h) = \frac{\varepsilon_L}{\phi} \quad (24)$$

where, A is a set of material constants and $B(T)$ is a set of temperature-dependent material properties.

For this implementation the formulation given in (9) is applied to (24), where, using the material constants given in Table 1, the full, temperature-dependent isotherms for the normal-strength (NSC) and high-performance concretes (HPC) under consideration are shown in Figure 5. In defining these curves, the evolution of porosity follows (11) as described above. The evolution of permeability follows (15) with A_D (5.2 for NSC & 5.0 for HPC) back calculated to fit published experimental results and found to correspond well with the results discussed in Section 4. Although less important in defining the curves it may be noted that initial parameter values were derived from the original papers cited above with intrinsic permeability again back calculated.

It may be noted that by taking into account the temperature-dependent properties of water the new formulation inherently predicts extremely low saturations as the temperature approaches the critical point of water and so, as a reasonable approximation, the formulation can be allowed to develop without a restriction in temperature range. This avoids any numerical issues that might be associated with switching or discontinuous functions and their derivatives.

a) 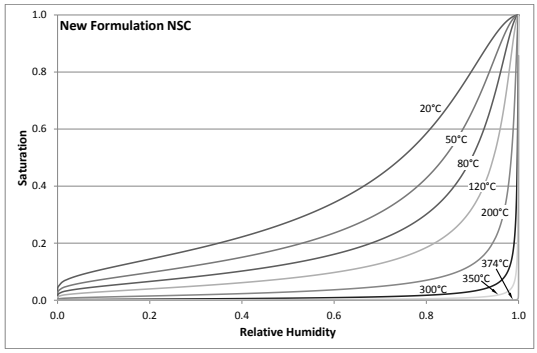

b) 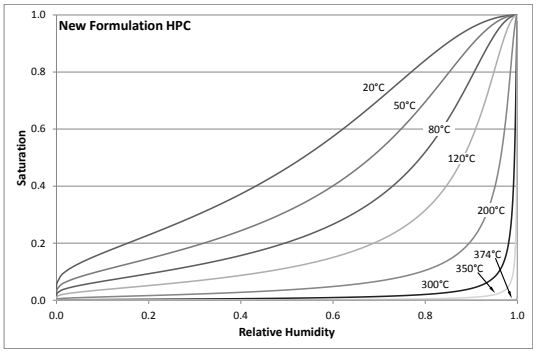

Figure 5 New formulation isotherms for a) normal-strength and b) high-performance concretes

For interest the equivalent plots of Bažant's isotherm formulation are shown below (Figure 6). The key parameter controlling the evolution of these curves with temperature is the cement content (See [11]) and this was derived from Kalifa et al. [32]. Other parameters were the same as for Figure 5. (It may be noted that the cement contents for the isothermal problem (taken from [17]) would be different but that this makes only a tiny difference to the 20°C curve with higher temperatures not relevant, so these are not shown here).

As can be seen, Bažant's curves are markedly different to the new formulation, especially at lower temperatures where, particularly for NSC they suggest much higher water contents through the mid-range of relative humidity, thereby implying a markedly different pore size distribution. The new formulation suggests more, larger pores that empty more quickly on drying. It is clear from Figure 4 above that Bažant's curves generally would not give a good fit for the measured isotherms and would not capture the variations seen for each different material. Poyet [16] suggested that this was partly because Bažant's curves were developed in order to cover a large range in temperature. But here we can see that the new formulation presents the opportunity to both capture the shapes of the measured isotherms and operate up to high temperatures.

It may also be noted that Bažant's formulation shows less difference between NSC and HPC, but also a reverse in trend over the new formulation, as for a given relative humidity, water content in HPC drops more rapidly with temperature than in NSC.

a) 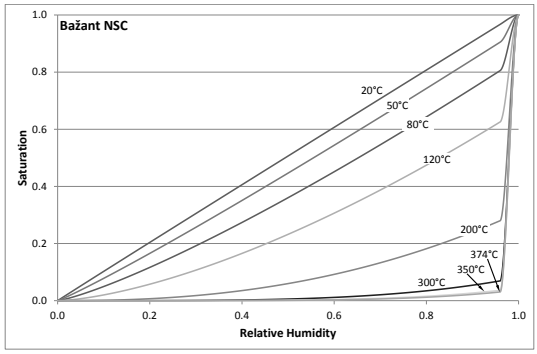

b) 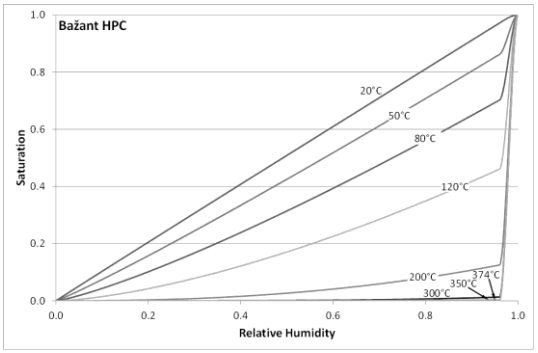

Figure 6 Bažant's formulation isotherms for a) normal-strength and b) high-performance concretes

5.1.3. Mechanical Constitutive Equations

While it can be shown that coupling of the fluid transport and mechanical behaviours of the concrete is critical to understanding the performance of the material under exposure to elevated temperatures [11] and indeed the sorption isotherms may be affected by the mechanical behaviour, the actual formulation of the mechanical component of the model is not critical to this work and so is not given a full treatment here. Briefly, a total strain formulation is developed ($\boldsymbol{\varepsilon}$) in which elastic strains ($\boldsymbol{\varepsilon}^e$), free thermal strains ($\boldsymbol{\varepsilon}^{ft}$) and load induced thermal strains ($\boldsymbol{\varepsilon}^{lits}$) are considered according to

$$\boldsymbol{\varepsilon} = \boldsymbol{\varepsilon}^e + \boldsymbol{\varepsilon}^{ft} + \boldsymbol{\varepsilon}^{lits} \tag{25}$$

The degradation of the concrete due to thermal and mechanical loading and the associated reduction of stiffness are accounted for by an isotropic scalar damage model where the Bishop's stress is given by

$$\boldsymbol{\sigma}' = (1-\omega)(1-\chi)\mathbf{D_0}:\boldsymbol{\varepsilon}^e \tag{26}$$

where, $\mathbf{D_0}$ is the initial elasticity tensor, ω is the mechanical damage parameter and χ is the thermal damage parameter.

5.1.4. Numerical Solution

A finite element implementation is employed, discretising the governing equations in space, with primary variables of displacements, $\boldsymbol{u}$, temperature, T, gas pressure, P_G, and vapour content, $\tilde{\rho}_V$. A generalised mid-point finite difference scheme is employed to discretise the problem in time. Boundary conditions for the temperature and vapour content are considered to be of the Cauchy (mixed) type, while a Dirichlet type (fixed) condition is assumed for the gas pressure (i.e. atmospheric pressure).

5.2. Numerical Examples

5.2.1. Baroghel-Bouny Isothermal Drying Problem

The model set up for the Baroghel-Bouny problem, representative of concrete cylinders 160mm in diameter and 100mm in length and undergoing uniaxial drying only from the ends of the samples, is shown in Figure 7 and Table 3 below.

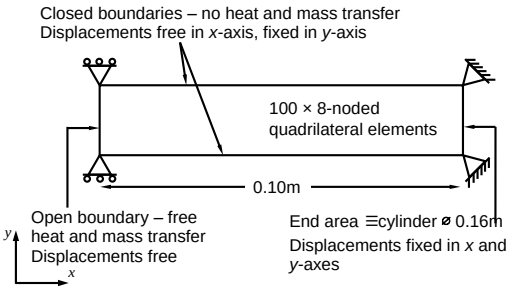

Figure 7 Model set up for Baroghel-Bouny isothermal drying problem

Table 3 Model Parameters for Baroghel-Bouny isothermal drying problem

	Value	
Parameter	NSC	HPC
Initial internal temperature, T	20°C	20°C
Initial internal gas pressure, P_G	101325Pa	101325Pa
Initial internal vapour content, $\tilde{\rho}_v$	0.016077kg/m^3	0.011064 kg/m^3
	≡~93%RH	≡~64%RH
External temperature, T	20°C	20°C
External gas pressure, P_G	101325Pa	101325Pa
External vapour content, $\tilde{\rho}_v$	50%RH	50%RH
Initial porosity	12.2%	8.2%
Initial permeability	4.2×10^{-21}m^2	2.5×10^{-21}m^2

As noted in the original work, this problem is near stress free and thus essentially hygro-thermal with little or no mechanical effects that might induce damage and affect the permeability.

Baroghel-Bouny et al. presented experimental results showing the mass losses and the relative density profiles across the samples over a period of approximately 1 year under exposure to controlled isothermal drying conditions [17]. The results of the numerical

analyses carried out using the new isotherm formulation are shown in comparison to the experimental results in Figures 8 & 9.

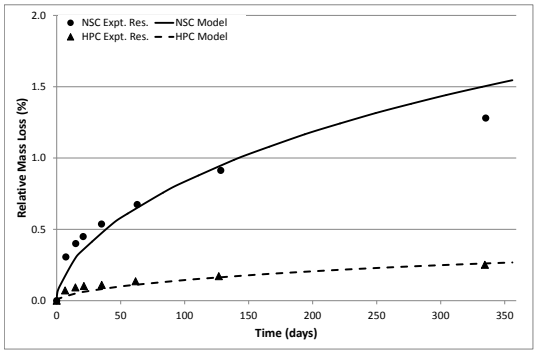

Figure 8 Mass loss in time from normal-strength and high-performance concretes

Generally it can be seen that the mass loss results follow the trend of the experimental results well. While the final mass loss for NSC is slightly over predicted this is similar to the trend shown by Baroghel-Bouny et al. [17] and to that seen using the Bažant formulation [11], and may suggest an effect more related to the transient flow aspects of the numerical models. It can also be noted that the mass loss for HPC is in fact better predicted than in those previous studies, suggesting a strong adaptability of the new isotherm formulation to different materials.

Furthermore, the relative density profiles predicted by the model (Figure 9a & b) can be seen to match well both across the sample length and in their development in time. Again, the significant difference in the behaviours of the NSC and HPC is captured well.

a) 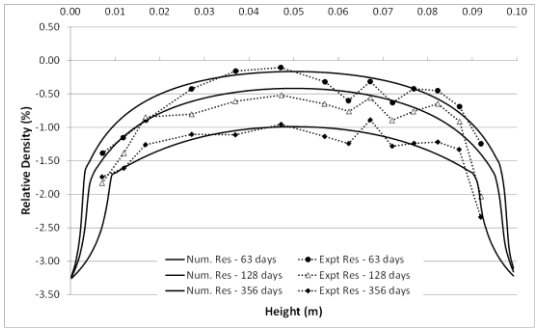

b) 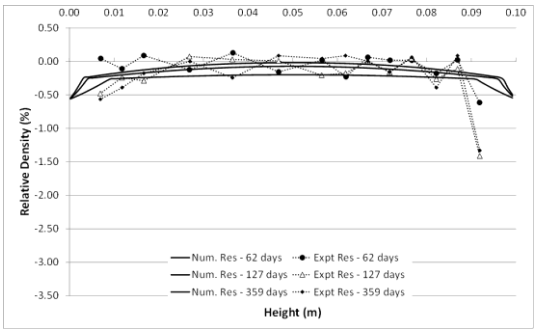

Figure 9 Moisture density profiles across a) normal-strength concrete sample and b) high-performance concrete sample

A further effect of note is that in order to best fit the transient drying results to the experimental results a different permeability is required when using the new formulation isotherms as compared to when using the Bažant formulation [11]; i.e. under transient drying

conditions the shape of the isotherm controls the evolution of water content in an apparently similar way to permeability (local equilibrium versus flow away from the region). The effect is less notable for HPC where the two isotherms are reasonably similar but is significant for NSC where there is a pronounced difference in the shape of the isotherms (Figures 4 & 5). Encouragingly, the permeability used in conjunction with the new isotherm formulation matches very closely the values reported by Baroghel-Bouny et al.

5.2.2. Kalifa High Temperature Problem

The model set up for the Kalifa high temperature problem, representative of concrete slabs 120mm thick and 300 × 300mm in plan area subjected to a temperature of 600°C on one face, is shown in Figure 10 and Table 4 below.

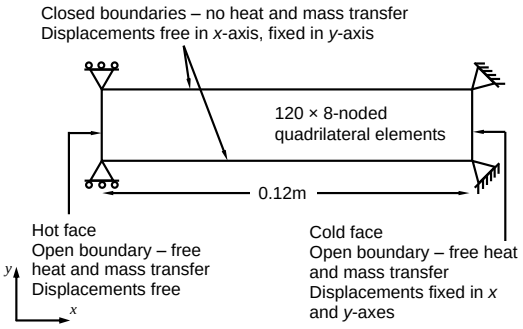

Figure 10 Model set up for Kalifa high temperature problem

Table 4 Model Parameters for Kalifa high temperature problem

Parameter	Value	
	NSC	HPC
Initial internal temperature, T	20°C	20°C
Initial internal gas pressure, P_G	101325Pa	101325Pa
Initial internal vapour content, $\tilde{\rho}_v$	0.014262kg/m^3 ≡~82.5%RH	0.013830 kg/m^3 ≡~80%RH
External hot face temperature, T	600°C	600°C
External hot face gas pressure, P_G	101325Pa	101325Pa
External hot face vapour content, $\tilde{\rho}_v$	0.05%RH	0.05%RH
External cold face temperature, T	25°C	25°C
External cold face gas pressure, P_G	101325Pa	101325Pa
External cold face vapour content, $\tilde{\rho}_v$	65%RH	65%RH
Initial porosity	14.3%	9.4%
Initial permeability	3.5×10^{-21}m^2	6.0×10^{-22}m^2

While this a high temperature scenario, the exposure of the concrete to a sudden and constant atmospheric temperature of 600°C results in a reasonably slow heating rate when compared, for example, to that produced by the ISO834 fire curve. This means that, although the concrete experiences rapid drying in the zone nearest the heat, it does not show the near vertical drying front (snapping from high relative humidity to near zero relative humidity) seen under fire loadings (See for example [10, 33, 34]) and so a range of relative humidity exists in the drying region of the concrete. Thus, the full range of the isotherms are tested by this experimental set-up.

Furthermore, although not overtly a thermo-mechanical problem, mechanical effects, especially the consideration of load induced thermal strains (LITS), have been shown to be critical in capturing the mass transport correctly in this problem [11]. Since LITS acts to dissipate stresses it limits the development of mechanical damage and the problem remains largely a hygro-thermal one.

Kalifa et al. presented experimental results showing the transient temperature and gas pressure profiles measured at various points through the thickness of the samples over a

period of 6 hours exposure to a fixed external atmospheric temperature of 600°C [32]. The results of the numerical analyses carried out using the new isotherm formulation are shown in comparison to the experimental results in Figure 11.

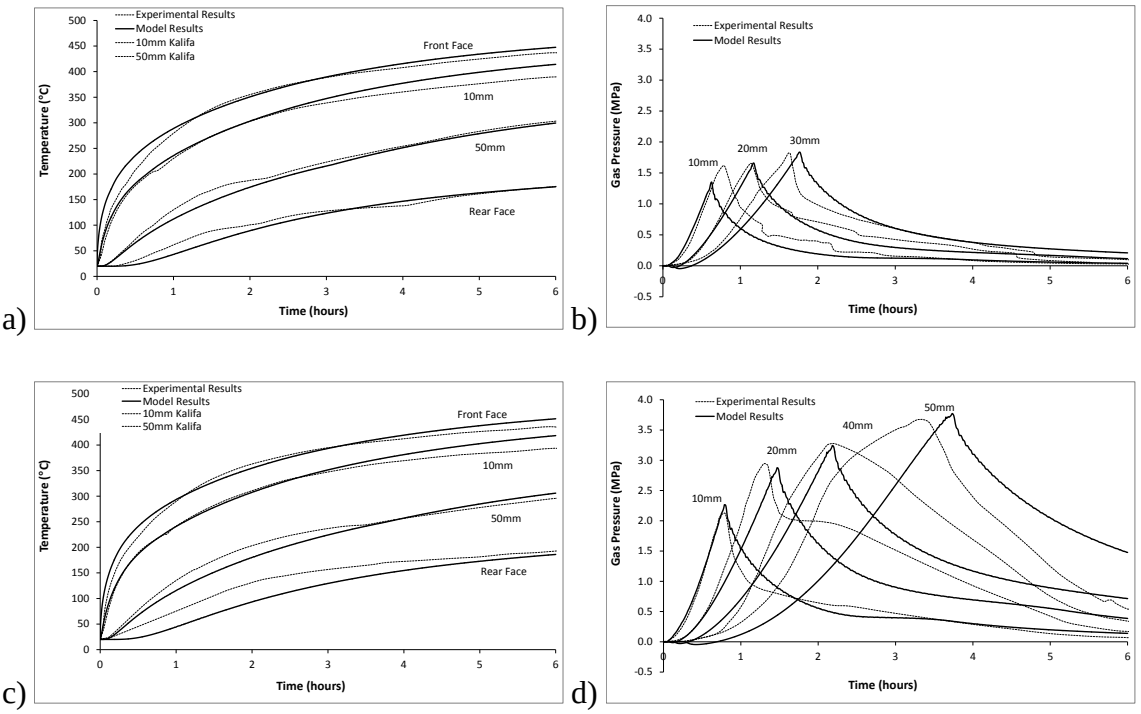

Figure 11 Temperature and gas pressure profiles in time for a) & b) normal-strength concrete (M30) and c) & d) high-performance concrete (M100)

As can be seen in Figures 11a & c, the temperature evolution throughout the specimens is predicted well for both NSC and HPC. Although not directly a function of the isotherm there is a strong coupling with temperature since the saturation of the concrete affects the thermal properties of conductivity and heat capacity and is also affected by phase change behaviours including evaporation of liquid water.

Importantly there are also good matches between the predicted and measured pore pressure evolutions in time at various points through the samples. Particularly in the NSC sample the timing, size and shape of the peaks match very well the experimental results. For the HPC sample the timing, size and shape of the first peak at 10mm is also very good, as are the timings and heights of the other peaks although it is noted that there are differences in the shape of the peaks in time. The reasons for this are not completely clear but similar issues are seen using the Bažant formulation and there may be experimental factors at work. However, it may also be noted that the gas pressure peaks produced by the new formulation show a rounding to their shape not seen when using the Bažant formulation [11].

As in the previous, isothermal example, the application of the Bažant formulation to this problem for NSC requires a different, higher, permeability in order to best fit the experimental results. This makes sense when it is considered that the Bažant formulation predicts a higher water content through the mid-range of relative humidity than the new formulation (Figures 5 & 6) and so a higher permeability is required to remove that water from the system and keep the gas pressures down to the measured values. Again, the difference is less pronounced for HPC where the isotherms are more similar.

6. Conclusions

To address the growing and significant need to understand, analyse and assess moisture transport in cementitious materials in safety critical applications such as nuclear reactor vessels, structures exposed to fire and well bore grouts, a rigorous and robust methodology has been presented to describe a formulation for temperature-dependent water retention curves (sorption isotherms), empirically based on the measured evolution of physical properties; porosity, permeability, surface tension and water density.

The model formulation was successfully validated for temperatures up to 80°C against independent sets of experimental data from Drouet et al. [24], Ishida et al. [25] and Brue et al. [26] as presented by Poyet [16]. Given a lack of experimental results above 80°C the model formulation was tested at higher temperatures through numerical reproduction of laboratory experiments following implementation in a fully coupled hygro-thermo-mechanical finite element model considering first an isothermal drying problem and then a high temperature problem. The new formulation was found to work well under a variety of conditions in a variety of cementitious material types and offers a consistent and robust method to account for changes in moisture content in these materials when exposed to elevated temperatures. It can be seen to offer versatility whereby it fits well with the shape and evolution of experimental isotherm measurements in the lower temperature ranges, while maintaining consistency with derived permeabilities, and at the same time extrapolates in a meaningful and consistent way to operate successfully at high temperatures.

7. References

[1] Z.P. Bažant, W. Thonguthai, Pore Pressure and Drying of Concrete at High Temperature, Journal of the Engineering Mechanics Division, ASME, 104 (1978) 1059 - 1079.
[2] Committee on Climate Change, The Renewable Energy Review, <http://www.theccc.org.uk/reports> Last accessed 28 Aug 2012, London, UK, 2011.
[3] Parliamentary Office of Science and Technology, Carbon Footprint of Electricity Generation, 2011.
[4] IAEA, Mission Report: The Great East Japan Earthquake Expert Mission - IAEA International Fact Finding Expert Mission of the Fukushima Dai-Ichi NPP Accident Following the Great East Japan Earthquake and Tsunami, IAEA, Division of Nuclear Installation Safety, Department of Nuclear Safety and Security, Tokyo, 2011.
[5] BP, Deepwater Horizon accident and response, http://www.bp.com/en_us/bp-us/commitment-to-the-gulf-of-mexico/deepwater-horizon-accident.html, 2014.
[6] G.L. England, N. Khoylou, Moisture Flow in Concrete Under Steady State Non-Uniform Temperature States: Experimental Observations and Theoretical Modelling, Nuclear Engineering Design, 156 (1995) 83 - 107.
[7] D. Gawin, C.E. Majorana, B.A. Schrefler, Numerical Analysis of Hygro-Thermal Behaviour and Damage of Concrete at High Temperature, Mech of Cohesive-Frictional Mat., 4 (1999) 37-74.
[8] J. Stabler, Computational Modelling of Thermo-mechanical Damage and Plasticity in Concrete, PhD Thesis, The University of Queensland, Australia., 2000.
[9] G.A. Khoury, C.E. Majorana, F. Pesavento, B.A. Schrefler, Modelling of Heated Concrete, Magazine of Concrete Research, 54 (2002) 77 - 101.
[10] R.T. Tenchev, L.Y. Li, J.A. Purkiss, Finite Element Analysis of Coupled Heat and Moisture Transfer in Concrete Subjected to Fire, Numerical Heat Transfer - A, 39 (2001) 685 - 710.
[11] C.T. Davie, C.J. Pearce, N. Bicanic, A Fully Generalised, Coupled, Multi-Phase, Hygro-Thermo-Mechanical Model for Concrete, Materials and Structures, 43 (2010).
[12] M.B. Dwaikat, V.K.R. Kodur, Hydrothermal model for predicting fire-induced spalling in concrete structural systems, Fire Safety Journal, 44 (2009) 425-434.
[13] T. Hozjan, M. Saje, S. Srpcic, I. Planinc, Fire analysis of steel-concrete composite beam with interlayer slip, Computers & Structures, 89 (2011) 189-200.
[14] M. Benes, R. Stefan, J. Zeman, Analysis of coupled transport phenomena in concrete at elevated temperatures, Applied Mathematics and Computation, 219 (2013) 7262-7274.
[15] Z.P. Bažant, M.F. Kaplan, Concrete at High Temperatures: Material Properties and Mathematical Models, Longman, Harlow, 1996.
[16] S. Poyet, Describing the influence of temperature on water retention using van Genuchten equation, Cement and Concrete Research, 84 (2016) 41-47.
[17] V. Baroghel-Bouny, M. Mainguy, T. Lassabatere, O. Coussy, Characterization and Identification of Equilibrium and Transfer Moisture Properties for Ordinary and High-Performance Cementitious Materials, CeM & Conc Res., 29 (1999) 1225-1238.
[18] M.T. van Genuchten, A Closed-form Equation for Predicting the Hydraulic Conductivity of Unsaturated Soils, Soil Science Society of America Journal, 44 (1980) 892-898.
[19] M.C. Leverett, Capillary behaviour in porous solids, Transactions of the American Institute of Mining and Metallurgical Engineers 1421941, pp. 152-169.
[20] D.J. Furbish, Fluid Physics in Geology: An Introduction to Fluid Motions on Earth's Surface and Within Its Crust, Oxford University Press1997.
[21] http://www.iapws.org/, The International Association for the Properties of Water and Steam.
[22] X. Luo, W. Sun, S.Y.N. Chan, Effect of heating and cooling regimes on residual strength and microstructure of normal strength and high-performance concrete, Cement and Concrete Research, 30 (2000) 379-383.
[23] C.T. Davie, C.J. Pearce, N. Bicanic, Aspects of Permeability in Modelling of Concrete Exposed to High Temperatures, Transport in Porous Media, 95 (2012) 627-646.

[24] E. Drouet, S. Poyet, J.M. Torrenti, Temperature influence on water transport in hardened cement pastes, Cement and Concrete Research, 76 (2015) 37-50.
[25] T. Ishida, K. Maekawa, T. Kishi, Enhanced modeling of moisture equilibrium and transport in cementitious materials under arbitrary temperature and relative humidity history, Cement and Concrete Research, 37 (2007) 565-578.
[26] F. Brue, C.A. Davy, F. Skoczylas, N. Burlion, X. Bourbon, Effect of temperature on the water retention properties of two high performance concretes, Cement and Concrete Research, 42 (2012) 384-396.
[27] D. Gawin, F. Pesavento, B.A. Schrefler, Simulation of damage-permeability coupling in hygro-thermo-mechanical analysis of concrete at high temperature, Communications in Numerical Methods in Engineering, 18 (2002) 113 - 119.
[28] C.V. Nielsen, C.J. Pearce, N. Bicanic, Improved phenomenological modelling of transient thermal strains for concrete at high temperatures, Computers and Concrete, 1(2) (2004) 189 - 209.
[29] S. Dal Pont, B.A. Schrefler, A. Ehrlacher, Intrinsic permeability evolution in high temperature concrete: An experimental and numerical analysis, Trans in Por Med., 60 (2005) 43-74.
[30] P. Kalifa, G. Chene, C. Galle, High-temperature behaviour of HPC with polypropylene fibres - From spalling to microstructure, Cem & Conc Res., 31 (2001) 1487-1499.
[31] U. Schneider, H.J. Herbst, Permeabilität und Porosität von Beton bei hohen Temperaturen, Deutschen Ausschuss für Stahlbeton, 403 (1989) 23 - 52.
[32] P. Kalifa, F.-D. Menneteau, D. Quenard, Spalling and Pore Pressure in HPC at High Temperatures, Cement and Concrete Research, 30 (2000) 1915 - 1927.
[33] C.T. Davie, C.J. Pearce, N. Bicanic, Coupled Heat and Moisture Transport in Concrete at Elevated Temperatures - Effects of Capillary Pressure and Adsorbed Water, Numerical Heat Transfer, Part A, 49 (2006) 733 - 763.
[34] D. Gawin, F. Pesavento, B.A. Schrefler, Modelling of Hygro-Thermal Behaviour and Damage of Concrete at Temperature above the Critical Point of Water, International Journal for Numerical and Analytical Methods in Geomechanics, 26 (2002) 537 - 562.